energies

MDPI

Article

Speed Fluctuation Suppression Based on an Adaptive Periodic Disturbance Observer for an Inverter Compressor

Fankun Meng [1], Zhengguo Li [2,*], Xiaoli Sun [2], Xiaoqin Wen [1], Michael Negnevitsky [3] and Linru You [1]

1 School of Automation Science and Engineering, South China University of Technology, Guangzhou 510641, China; josephmeng@163.com (F.M.); xqwen@scut.edu.cn (X.W.); aulryou@163.com (L.Y.)
2 School of Automobile and Transportation, Shenzhen Polytechnic, Shenzhen 518055, China; sunxiaoli@szpt.edu.cn
3 School of Engineering, College of Science and Engineering, University of Tasmania, Tasmania 7001, Australia; Michael.Negnevitsky@utas.edu.au
* Correspondence: lizhengguo@szpt.edu.cn; Tel.: +86-131-2953-5796

Received: 12 July 2020; Accepted: 27 August 2020; Published: 24 September 2020

Abstract: Repetitive operations have been extensively used in the inverter compressor refrigeration industry. The approximately periodic disturbance caused by repetitive operations must be compensated to realize stable and high-efficiency operation. In this paper, a periodic disturbance observer (PDOB) is proposed to tackle the speed fluctuation of an inverter compressor in the low-frequency range. Periodic disturbance, consisting of a fundamental wave and corresponding harmonics, can thus be estimated and compensated; in addition, sensitivity and complementary sensitivity can reach a compromise through the use of a certain parameter. Aiming at a different operation environment, an adaptive notch filter based on the Steiglitz–McBride method is employed to estimate the fundamental frequency of periodic disturbance. Finally, the feasibility of our approach is verified by MATLAB simulation, and experiments are implemented to illustrate that speed fluctuation can be more effectively attenuated by the proposed method in comparison with general DOB.

Keywords: periodic disturbance observer; inverter compressor; speed fluctuation; frequency adaptiveness

1. Introduction

Owing to its small size, simple structure, high power density and efficiency characteristics, induction motor (IM) has been gradually substituted by permanent magnetic synchronous motor (PMSM) in inverter compressor refrigeration industry [1,2]. An approximately periodic pressure gap between the evaporator and condenser caused by repetitive operations is widely present for inverter compressors; in addition, the approximately periodic pressure gap caused by repetitive operation deteriorates its normal operation performance, with negative characteristics such as speed fluctuation, current distortion, self-commissioning failure, noise and vibration, etc. In the process of realizing stable operation with a high energy efficiency ratio (EER), speed fluctuations caused by periodic disturbance in the low-frequency range are a critical problem.

In order to suppress speed fluctuation in the low-frequency range and the corresponding issues caused by periodic disturbance, extensive research has been conducted, and some effective methods have been implemented. At present, sinusoidal wave torque compensation is widely employed in engineering applications, which neglects aperiodic and high-order harmonic components of periodic disturbance; consequently, load torque cannot be effectively compensated, and a speed fluctuation

occurs. Zhang et al. [1], in the Midea group, adopted Fourier transformation to extract the speed fluctuation and deduce the current compensation to suppress speed fluctuation in low-frequency range, showing that their approach could efficiently reduce speed fluctuation; however, the speed fluctuation suppression effect is variable according to the operation environment, especially the pressure gap between the evaporator and condenser. Huang et al. [2], in the Gree group, proposed a method which can automatically realize load torque compensation, which is essentially a general disturbance observer (DOB) and neglects the influence of harmonic components of disturbance. Both of the above methods neglect harmonic components of periodic disturbance; consequently, the performance of periodic disturbance suppression is finite, and the speed fluctuation is comparably obvious in the low-frequency range.

Generally, disturbances are extensively present in inverter compressor control system, such as parameter variation, unmodeled dynamics, frictional resistance and load torque disturbance, etc., which have adverse effects on control performance; in particular, the control system may be unstable. Compared with conventional feedback control, disturbance compensation can directly and effectively suppress disturbance. However, quite often, the disturbance cannot be directly measured by the sensor or is too complicated to implement; therefore, a large amount of disturbance/uncertainty estimation and attenuation (DUEA) [3] techniques have been proposed. In this area, the disturbance observer (DOB) [4] and extended state observer (ESO) [5] have been extensively employed for disturbance compensation.

The disturbance observer (DOB) [4] is an effective method to suppress disturbance which was originally proposed by Ohnishi; improvements were made to the approach later, such as repetitive DOB (RDOB) [6], fuzzy DOB (FDOB) [7], etc. DOB is essentially a two-degree-of-freedom controller based on an observer structure used to suppress disturbance [8], which can realize disturbance suppression and not influence the reference command tracking ability. The kernel part of DOB is a filter which determines the sensitivity function and the complementary sensitivity function of DOB. Generally, a low-pass filter is employed to realize high-pass sensitivity and low-pass complementary sensitivity characteristics on the basis of a compromise between the functions, because the sensitivity function represents disturbance suppression performance and the complementary sensitivity function represents noise sensitivity and robust stability [4]. However, the high-pass characteristic is incapable of compensating for periodic disturbance because it possesses power only at an infinite amount of harmonic frequency. Therefore, in order to suppress periodic disturbance, research works concerning DOB and high-order DOBs have been implemented for some specific high-frequency harmonics; however, the complicated design procedure makes this difficult to implement for practical application. In [5], a periodic learning disturbance observer was proposed which consisted of searching and learning phases, in which a general DOB was adopted in searching phase stage; however, this did not take advantage of DOB characteristics in the learning phase, and therefore this method (which also influenced tracking characteristic) was not a two-degree-of-freedom controller—rather, it was more similar to a repetitive controller (RC) than a DOB.

The extended state observer (ESO) is an effective method to suppress disturbance and was originally proposed by Han et al. [9]; it is a fundamental part of active disturbance rejection control (ADRC) and is employed to estimate the lumped disturbance including uncertainty and external disturbance, etc. However, ADRC has the following disadvantages [10]: firstly, it is difficult to select the relative order for a non-minimum phase system; secondly, tuning the bandwidth parameters of ESO to achieve satisfactory characteristics under practical restrictions is complicated; thirdly, large numbers of nonlinear strategies are adopted in the original ADRC, which complicates control system design.

The repetitive controller (RC) was originally proposed by Nakano et al. [11] according to the internal model theorem [12]; owing to its simple structure and easy implementation, it has been extensively employed for periodic signal tracking or suppression [13–15]. However, RCs have the following disadvantages [16]: firstly, the phase delay item deteriorates control system stability; secondly, the sensitivity gain drops at aperiodic components cause decreases in the disturbance

suppression characteristics; thirdly, the robustness against measurement noise and unmodeled dynamics is reduced [17]; fourthly, a large amount of memory space is required to store previous values when the period of the disturbance signal is long. An RC based on DOB was proposed in [6]; even though disturbance was effectively attenuated, the bandwidth characteristics of the sensitivity function suppressing harmonic disturbance were narrow, while the command tracking characteristic and system stability were still influenced by the phase delay item. In order to solve this problem, a phase lead item was adopted in [18] to compensate phase delay. An finite impulse response (FIR) filter was adopted in [19] to realize fractional delay compensation, substituting a low-pass filter (LPF) by altering corresponding coefficients; however, this approach is inappropriate when a system has high-frequency disturbance, such as under model uncertainties and parameter variation, etc. The use of Lagrange series expansion to approximate fractional delay (FD) was proposed in [20], in contrast to general RC, which can theoretically suppress any frequency disturbance; however, high-frequency disturbance cannot be suppressed effectively because of the amplitude fluctuation and phase delay. In addition, disturbance suppression precision and the dynamic response of harmonic suppression should be comprehensively taken into consideration.

In this paper, a periodic disturbance observer (PODB) is adopted to resolve the speed fluctuation of an inverter compressor, especially in the low-frequency range, which solves the above-mentioned problems. Firstly, the system stability and disturbance suppression characteristics are not influenced by the phase lag item; secondly, a zero phase delay low pass filter is introduced into the PDOB, which is employed to reach a compromise between sensitivity and complementary sensitivity; thirdly, the magnitude gain of other aperiodic disturbances can be attenuated by a certain parameter—meanwhile, the complementary sensitivity function can also be regulated.

Compared with general DOB, PDOB can estimate and compensate periodic disturbance more effectively because a periodic disturbance internal model is adopted to represent the band pass characteristic (a large magnitude gain at harmonic frequencies can be employed for periodic disturbance compensation); however, general DOB only has a low pass characteristic (a finite magnitude gain at harmonic frequencies, and it cannot be employed for periodic disturbance compensation). Furthermore, the band-pass characteristic of PDOB at harmonic frequencies can achieve better periodic disturbance suppression performance than other conventional disturbance suppression methods, such as active disturbance rejection control [10] and general DOB [4].

Moreover, periodic disturbance suppression performance varies with the operation environment of the inverter compressor refrigerating system; in particular, a closed loop system may be unstable, and therefore adaptive fundamental frequency estimation is adopted to tackle this problem [21,22]. As the adaptive notch filter (ANF) is widely adopted in signal processing [21,23], such as signal separation and enhancement, ANF based on the Steiglitz–McBride (SM) [24] method is employed to estimate the fundamental frequency from periodic disturbance including the fundamental components and corresponding harmonics.

Aiming at the speed fluctuation of inverter compressors in the low-frequency range, adaptive PDOB is employed to realize disturbance estimation and current compensation. This paper is organized as follows: firstly, a model of the inverter compressor driving system is constructed, and necessary assumptions are made to simplify the analysis and design; secondly, PDOB is proposed, and a detailed design procedure of the corresponding parameters is presented; thirdly, ANF based on the SM method is employed to realize fundamental wave frequency estimation; finally, MATLAB simulations (2013b, MathWorks, MA, USA) and experiments are presented to verify the feasibility and effectiveness of adaptive PDOB.

2. Modeling and Analysis

2.1. Model Introduction

The structural diagram of a single rotor inverter compressor is presented in Figure 1a; the key parts are the rotor and bump, presented in Figure 1b. The bump primarily consists of a cylinder, crankshaft, piston, upper and lower bearing, etc., where machinery precision and cooperation determine the performance and durability of the inverter compressor. Figure 1c is the rotating inverter compressor operation cycle, where A denotes the left volume intake, B denotes the left volume close and air compression, C denotes left volume compression along with right volume intake, D denotes the left volume exhaust along with right volume intake, E denotes the left volume exhaust along with right volume intake and F denotes the right volume exhaust along with a new B procedure. As the cylinder is divided into left and right volumes by a slider block and eccentric piston, the cyclic operation procedure, including intake, compression and exhaust, makes the air pressure gap approximately periodic; that is, the load of the inverter compressor will present approximately periodic variation. Figure 2 denotes inverter compressor load torque waveforms under different operation environments [2]. It can be observed that the load torque is approximately periodic; meanwhile, the magnitude and phase are different from each other under different operation environments.

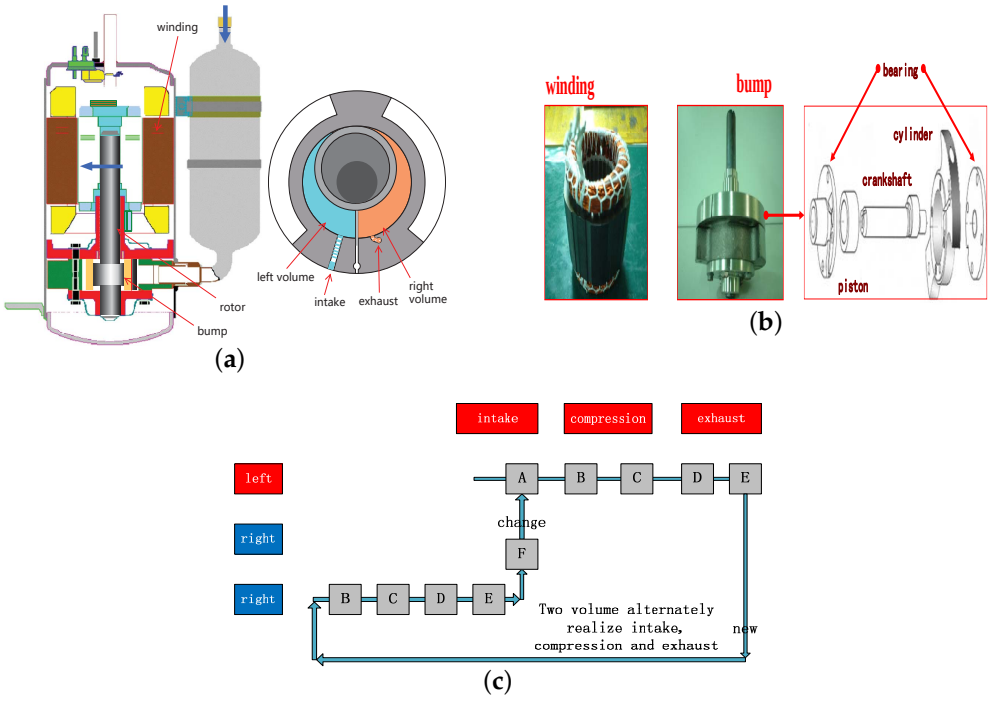

Figure 1. Structural diagram of the inverter compressor and operating procedure: (**a**) inverter compressor structure diagram; (**b**) winding and bump; (**c**) operation cycle.

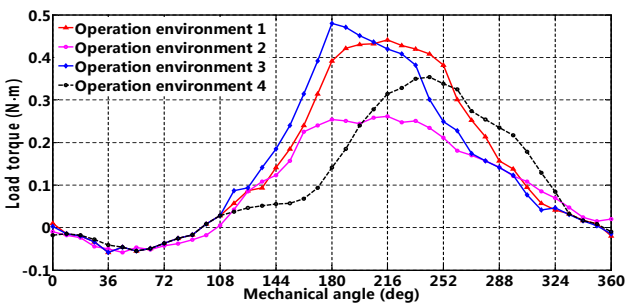

Figure 2. Load torque under different operation environments.

The simplified control block diagram of the inverter compressor driving system with general DOB is presented in Figure 3, where ω_{ref} and ω_r denote the speed reference and feedback value, respectively, i_{ref} and i_r denote the torque current reference and feedback value, respectively, i_d denotes the current compensation obtained from general DOB, K_{Tn} and K_T denote the nominal and real electromagnetic torque constant, respectively, K_v denotes the back electromagnetic force (EMF) constant, T_d denotes the load torque, J_n and J denote the nominal and real moment of inertia, respectively, n denotes the measurement noise and g denotes the cutoff frequency of the LPF. For a slow variance or constant disturbance, a compromise between sensitivity and complementary sensitivity can be achieved by using a proper cutoff frequency; consequently, disturbance can be effectively compensated and speed fluctuation can be asymptotically rejected in a steady state.

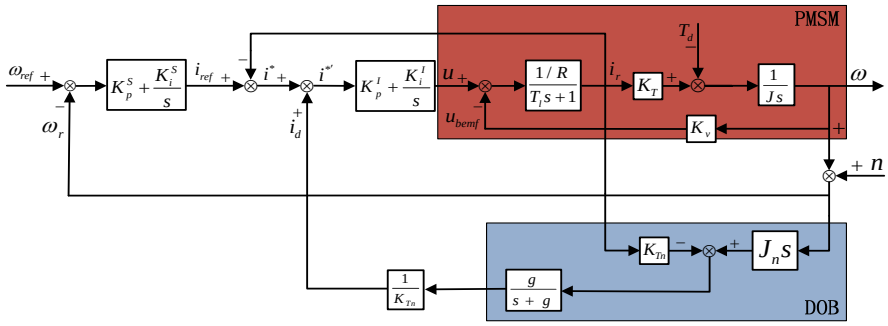

Figure 3. Simplified control block diagram of an inverter compressor with a general disturbance observer (DOB).

We suppose that (1) the rotor core is without saturation, (2) eddy current loss is not considered and (3) the flux caused by the phase current and rotor permanent magnet presents sinusoidal distribution. Under a synchronously rotating d-q coordinate, the inverter compressor rotating equation can be derived as follows.

$$\begin{cases} J_n\ddot{\theta} = T_e - B\dot{\theta} - T_d \\ T_e = \dfrac{3}{2}n_p\left[\psi_m i_q + (l_d - l_q)i_d i_q\right] \approx K_T i_q \\ T_d = -\Delta J\ddot{\theta} - T_r - T_{um} - T_l \\ K_T = \dfrac{3}{2}n_p\psi_m \end{cases} \tag{1}$$

where i_d and i_q denote the d-q axis current, respectively, l_d and l_q denote the d-q axis inductance, respectively, θ denotes the rotor mechanical angle, T_e and T_d denote the electromagnetic and load torque, respectively, J and B denote the equivalent moment of inertia and viscous damping coefficient, respectively, n_p denotes tbe number of pole pairs, ψ_m denotes the rotor equivalent permanent flux and T_d denotes the lumped torque including torque ripple, parameter variation and unmodeled dynamics, etc. $\Delta J = J - J_n$ denotes the parametric offset of equivalent moment of inertia, while T_r, T_l and T_{um} denote the torque ripple, basic load torque and unmodeled dynamic torque, respectively.

2.2. Assumptions and Properties

The control objective of this paper is to track the reference velocity ω_{ref} for an inverter compressor with minimized tracking error; meanwhile, the following assumptions [5] are necessary to simplify control system analysis and design for an inverter compressor driving system.

- Assumption 1: The influence of approximately periodic disturbance on the inverter compressor is almost identical under the same operation environment.
- Assumption 2: The control objective is speed fluctuation suppression under the same, repetitive operation environment.

- Assumption 3: Measurement noise is primarily present in the high-frequency range.

Supposing that disturbance satisfies the monic differential equation, as follows,

$$p^{n_d} d(t) + \sum_{i=1}^{n_d} \lambda_{n_d - i} p^{n_d - i} d(t) = 0 \tag{2}$$

where $p^{n_d - i}$ represents the $n_d - i$ order differential operator and $i = 1, \cdots, n_d$, $\lambda_{n_d - i}$ represents the corresponding coefficient, by Laplacian transformation, the following can be obtained:

$$\underbrace{\left[s^{n_d} + \lambda_{n_d - 1} s^{n_d - 1} + \cdots + \lambda_0\right]}_{\Gamma_d(s)} d(s) = f(0, s) \tag{3}$$

where $f(0, s)$ is the initial state of $d(t)$ which is determined by the corresponding initial state (e.g., $d(0)$, $\dot{d}(0)$, $\ddot{d}(0)$, $\cdots$) and $\Gamma_d(s)$ is the disturbance characteristic polynomial. Supposing that $d(t)$ is a periodic signal, then discrete expression can be written as follows;

$$d(k) = d(k - N) + f(k) \tag{4}$$

where

$$f(k) = \begin{cases} f_0(k) & k < N \\ 0 & N \leq k \end{cases} \tag{5}$$

where $f_0(k)$ and N are the initial value and periodic delay of $d(t)$, respectively. Therefore, a discrete transformation of periodic disturbance can be derived as follows.

$$d(z^{-1}) = \frac{1}{1 - z^{-N}} f(z^{-1}) \tag{6}$$

The control block diagram and the equivalent form of a general DOB are presented in Figure 4, where r, n, y, u, P, P_n, Q, d, $\hat{d}$, m and Δ denote the reference input, noise, output, controller, plant, nominal plant, Q filter to be designed, disturbance, disturbance estimation, relative degree of P and uncertain modeling error, respectively; $C(z^{-1})$ is an existing controller designed by the loop shaping method (e.g., proportional-integral-differential (PID) or H_∞) to realize servo performance or robustness. In Figure 4a, the sensitivity function can be obtained (for the sake of brevity, the discrete domain delay operator z^{-1} is omitted here).

$$S(z^{-1}) = \frac{1 - Qz^{-m}}{1 + PCz^{-m} + (PP_n^{-1} - 1)Qz^{-m}} \tag{7}$$

Note that the frequency characteristic of $P(e^{-j\omega})$ is approximate to that of $P_n(e^{-j\omega})$ in the low-frequency range; thus, the sensitivity function in Equation (7) can be written as follows:

$$S(z^{-1}) \approx \frac{1 - Qz^{-m}}{1 + PCz^{-m}} \tag{8}$$

Generally, large unmodeled dynamics are present in the high-frequency range, and the frequency characteristic of Q should make Equation (8) a valid approximation to Equation (7). Supposing that the periodic disturbance $d(t)$ satisfies the periodic disturbance polynomial characteristic—that is, if the term $1 - z^{-N}$ is incorporated into the numerator of Equation (7)—then periodic disturbance error

can asymptotically approach zero in the steady state. In this paper, an infinite impulse response (IIR) filter $Q = B_Q/A_Q$ is adopted, and we define $A_Q(z^{-1}) = 1 - \alpha^N z^{-N}$ [6]; then, B_Q satisfies

$$1 - \alpha^N z^{-N} - z^{-m} B_Q = \gamma(1 - z^{-N}) \tag{9}$$

Through simple calculation yielding $B_Q(z^{-1}) = (1-\gamma) - (\alpha^N - \gamma)z^{-N}$, where parameter γ will be designed later and z^{-m} is ignored to make Q a causal filter, the Q filter can consequently be derived as follows:

$$Q(z^{-1}) = \frac{(1-\gamma) - (\alpha^N - \gamma)z^{-N}}{1 - \alpha^N z^{-N}} \tag{10}$$

$$1 - Q(z^{-1}) = \frac{\gamma(1 - z^{-N})}{1 - \alpha^N z^{-N}} \tag{11}$$

Therefore, the periodic disturbance polynomial characteristic $1 - z^{-N}$ is incorporated into the numerator of Equation (7), which can guarantee that the steady-state error of periodic disturbance asymptotically converges to zero.

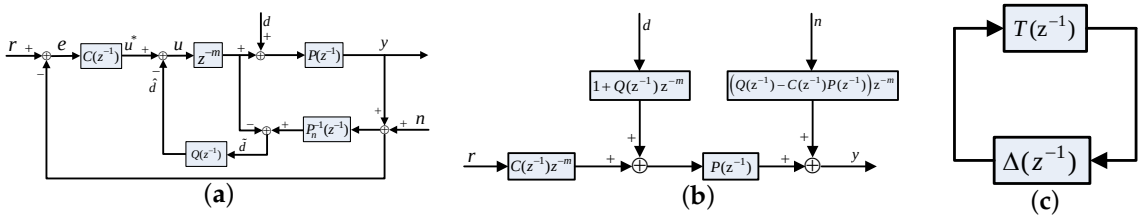

Figure 4. Control block diagram with general DOB: (**a**) block diagram of general DOB; (**b**) equivalent block diagram of DOB when $\Delta(z^{-1}) = 0$; (**c**) robust stability based on the small gain theorem.

3. Parameter Design

3.1. Nominal Stability

The nine transfer functions concerning r, d and n to y, u and $\hat{d}$ are presented in Equation (12), where the nominal plant P_n, Q filter and existing controller C can be expressed by the fractional coprime polynomials N_p/D_p, N_Q/D_Q and N_c/D_c, respectively; in addition, modeling uncertainty is primarily constituted by multiplicative error and $\Delta(z^{-1})$ is defined as $P(z^{-1}) = (1 + \Delta(z^{-1}))P_n(z^{-1})$. Consequently, the corresponding transfer functions can be derived as follows [25]:

$$\begin{bmatrix} y \\ u \\ \hat{d} \end{bmatrix} = \begin{bmatrix} N_p^2 N_c D_Q (1+\Delta) z^{-m} & N_p^2 D_c (D_Q + N_Q z^{-m})(1+\Delta) & -D_p N_p D_c N_Q (1+\Delta) \\ D_p N_p N_c D_Q & -N_p^2 N_c D_Q (1+\Delta) + D_p N_p D_c N_Q & -D_p^2 D_c N_Q \\ D_p N_p N_c N_Q \Delta z^{-m} & D_p N_p D_c N_Q (1+\Delta) & -D_p N_Q \left(D_p D_c + (1+\Delta) N_p N_c z^{-m}\right) \end{bmatrix} \begin{bmatrix} r \\ d \\ n \end{bmatrix} \frac{1}{DEN}$$

$$DEN = N_p \left(D_p D_c D_Q + N_p N_c D_Q (1+\Delta) z^{-m} + D_p D_c N_Q \Delta z^{-m}\right) \tag{12}$$

In Equation (12), when $\Delta(z^{-1}) = 0$, the characteristic polynomial can be rewritten as follows:

$$DEN = N_p D_Q \left(D_p D_c + N_p N_c z^{-m}\right) \tag{13}$$

Because the numerator and denominator of Q filter are coprime polynomials, then the nominal stability of PDOB depends on these items: zeros of nominal plant N_p, poles of nominal plant D_p,

poles of controller D_c and zeros of controller N_c. It can be observed that the nominal plant is uncorrelated to delay item z^{-N}; in other words, the nominal stability of the control system with PDOB is not influenced by the delay item z^{-N}.

3.2. Parameter α Design

$\alpha \in [0,1]$ is the ratio of poles and zeros in $1 - z^{-m}Q(z^{-1})$. If $\alpha = 0$, then $Q(z^{-1})$ becomes a finite impulse response (FIR) filter z^{-N+m}; if $\alpha = 1$, disturbance compensation, including periodic and aperiodic compensation, is broken off. When $\alpha \in (0,1)$, loop shaping can be designed with flexibility. The magnitude gains of $1 - Q(z^{-1})z^{-m}$ and $Q(z^{-1})$ are presented in Figure 5, where the corresponding parameters are $N = 200$, $T_s = 0.1$ ms, $m = 1$ and $\gamma = 1$. In Figure 5a, it can be observed that $1 - z^{-m}Q(z^{-1})$ presents a sharper comb-like shape with α decreasing to 0.1, where the maximum magnitude gain of $1 - Q(z^{-1})z^{-m}$ is equal to 2; that is, the magnitude gain of the corresponding frequency disturbance will be amplified by 100%. Similarly, in Figure 5b, $Q(z^{-1})$ behaves as a spectral selection filter to filter out specific frequency components of disturbance, such as 500, 1000, 1500, 2000 rad/s, etc., which can be employed to realize specific periodic disturbance compensation. Specifically, when $\alpha = 0.1$, the magnitude gain of $Q(z^{-1})$ is always equal to 1; that is, all periodic and aperiodic disturbance components are directly employed for disturbance compensation.

From the analyses of parameter α, it can be determined that transient overshoot and steady state performance conflict with each other. In order to reduce the possible overshoot or amplification of aperiodic components, a time-varying α is adopted for transient process improvement. It is proposed to initialize α_k and gradually increase it at the geometric ratio $\alpha_r \in (0,1)$ to an ultimate value of α_∞ following the rule $\alpha_{k+1} = \alpha_r\alpha_k + (1 - \alpha_r)\alpha_\infty$. The settling time of the Q filter is determined by the pole location of the filter. It can be clearly seen that the larger the term α^N, the longer the settling time; specifically, in the case of $\alpha = 0$, the settling time is short and can be neglected.

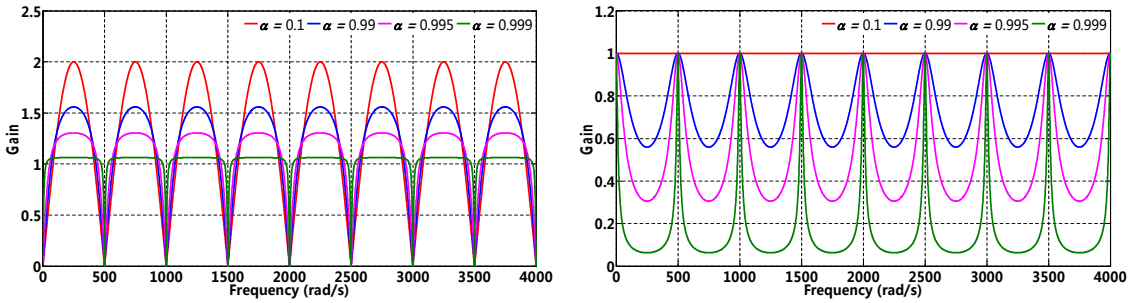

Figure 5. Magnitude gain waveforms with respect to parameter α: (**a**) $1 - Q(z^{-1})z^{-m}$; (**b**) $Q(z^{-1})$.

3.3. $q(z^{-1})$ Design

Generally, it is impossible to have an accurate model of $P(z^{-1})$ in the high-frequency range when model uncertainties are widely present. In order to implement a robust Q filter, a low-pass filter is employed to make the gain of $[PP_n^{-1} - 1]Qz^{-m}$ small, as shown in Equation (10). We define a zero-phase low-pass filter (ZPF) as follows [6]:

$$\begin{aligned} q(z^{-1}, z) &= q(z^{-1})q(z) \\ q(z^{-1}) &= \frac{1 - 2\cos(gT_s)z^{-1} + z^{-2}}{2 - 2\cos(gT_s)} \end{aligned} \tag{14}$$

where $q(z^{-1})$ and $q(z)$ are conjugates of each other and g is the cutoff frequency. The filter $q(z^{-1}, z)$ has four zeros at $e^{\pm gT_s}$ and is normalized by $(2 - 2\cos(gT_s))^2$ to have a unity direct current (DC) gain. Therefore, a robust implementation of the Q filter can be derived as follows:

$$Q(z^{-1}) = \frac{(1-\gamma) - (\alpha^N - \gamma)z^{-N}}{1 - \alpha^N z^{-N}} q(z^{-1}, z) \tag{15}$$

The effects of the zero-phase low-pass filter $q(z^{-1}, z)$ are presented in Figure 6. The corresponding parameters are $N = 2\pi/(\omega_0 T_s)$, $\omega_0 = 60$ rad/s, $\gamma = 0.5$, $T_s = 0.1$ ms, $g = 2000$ rad/s and $m = 1$, respectively. The periodic disturbance sensitivity and robust stability reach a compromise with each other. In Figure 6a, it can be observed that the magnitude gain of the sensitivity function is large in the low-frequency range, which illustrates that PDOB can suppress harmonic components primarily in the low-frequency range, while in the high-frequency range, the energy of harmonics and measurement noise is generally comparably weak, and the magnitude gain gradually increasing to 0 dB improves the robustness of the performance of PDOB. Meanwhile, the phase delay of PDOB with ZPF gradually converges to 0° while that of PDOB with $q(j\omega) = 1$ varies between −90° and 90°. In Figure 6b, harmonic components in the low-frequency range are implemented for disturbance compensation, while in the high-frequency range, the magnitude gain of the harmonics and measurement noise can be further attenuated to guarantee robust stability; meanwhile, the phase delay of PDOB with ZPF is same as that of PDOB with $q(j\omega) = 1$.

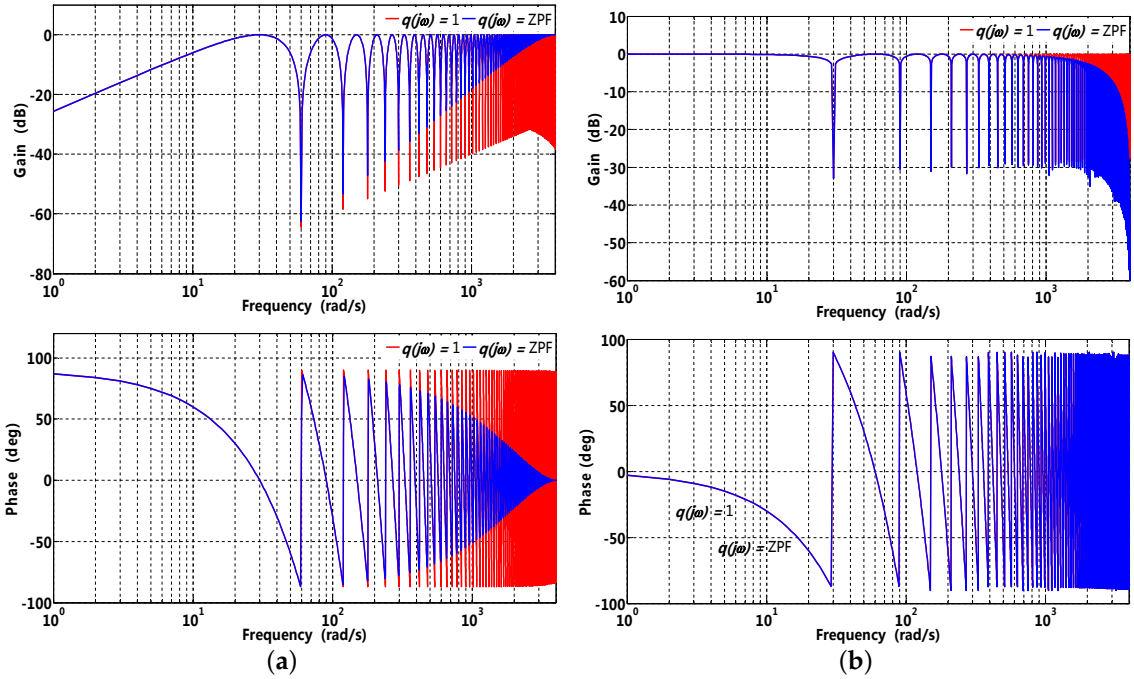

Figure 6. Frequency characteristics with respect to the low-pass filter (LPF): (**a**) $1 - Q(z^{-1})z^{-m}$; (**b**) $Q(z^{-1})$.

3.4. Parameter γ Design

The disturbance suppression performance of PDOB is primarily determined by the magnitude gain of the sensitivity function presented in Equation (7). In order to simplify our analyses, we primarily focus on the magnitude gain of Equation (11) as follows.

$$\left| \frac{\gamma(1 - z^{-N})}{1 - \alpha^N z^{-N}} \right| = \gamma \sqrt{\frac{1 - \cos(\omega_0 N)}{\frac{1+\alpha^{2N}}{2} - \alpha^N \cos(\omega_0 N)}} \tag{16}$$

where $\omega_0 = 2\pi f_0 T_s$ is fundamental frequency of periodic disturbance. After some simple calculation, it can be found that Equation (16) is a monotonic decreasing function with respect to $\cos(\omega_0 N)$—when $\cos(\omega_0 N) = 1$, Equation (16) has the minimum value of 0—in contrast, when $\cos(\omega_0 N) = -1$, Equation (16) has the maximum value of

$$\left|\frac{\gamma(1-z^{-N})}{1-\alpha^N z^{-N}}\right|_{max} = \frac{2\gamma}{1+\alpha^N} \approx 2\gamma \tag{17}$$

It can be observed that parameter γ influences the magnitude gain of Equation (11) at these frequencies, which corresponds to different disturbance suppression performances [8].

$$\omega_1 = (2n)\frac{\omega_0}{2},\ \omega_2 = (2n+1)\frac{\omega_0}{2},\ n = 1, 2, \cdots \tag{18}$$

The delay item z^{-m} is ignored to simplify the design of the parameter γ, and the magnitude gain of Equations (10) and (11) can be derived as follows:

$$\begin{aligned}\left|1 - Q(e^{-j\omega T_s})\right| &= \left|2\gamma \sin\left(-\frac{NT_s}{2}\omega\right)\right| \\ \left|Q(e^{-j\omega T_s})\right| &= \left|\sqrt{1 + 4\gamma(\gamma-1)\sin^2\left(-\frac{NT_s}{2}\omega\right)}\right|\end{aligned} \tag{19}$$

Substituting ω_1 and ω_2 into Equation (19), the following can be obtained.

$$\begin{aligned}\left|1 - Q(e^{-j\omega_1 T_s})\right| = 0,\ \left|1 - Q(e^{-j\omega_2 T_s})\right| &= |2\gamma| \\ \left|Q(e^{-j\omega_1 T_s})\right| = 1,\ \left|Q(e^{-j\omega_2 T_s})\right| &= |1 - 2\gamma|\end{aligned} \tag{20}$$

The frequency characteristics of Equations (11) and (10) with respect to parameter γ are presented in Figure 7, where the corresponding parameters are $T_s = 0.1$ ms, $N = 2\pi/(\omega_0 T_s)$, $\omega_0 = 60$ rad/s and $\alpha = 0.995$, respectively. Considering the optimal sensitivity and complementary sensitivity characteristic of Equations (11) and (10), γ is selected as 0.5 in this paper.

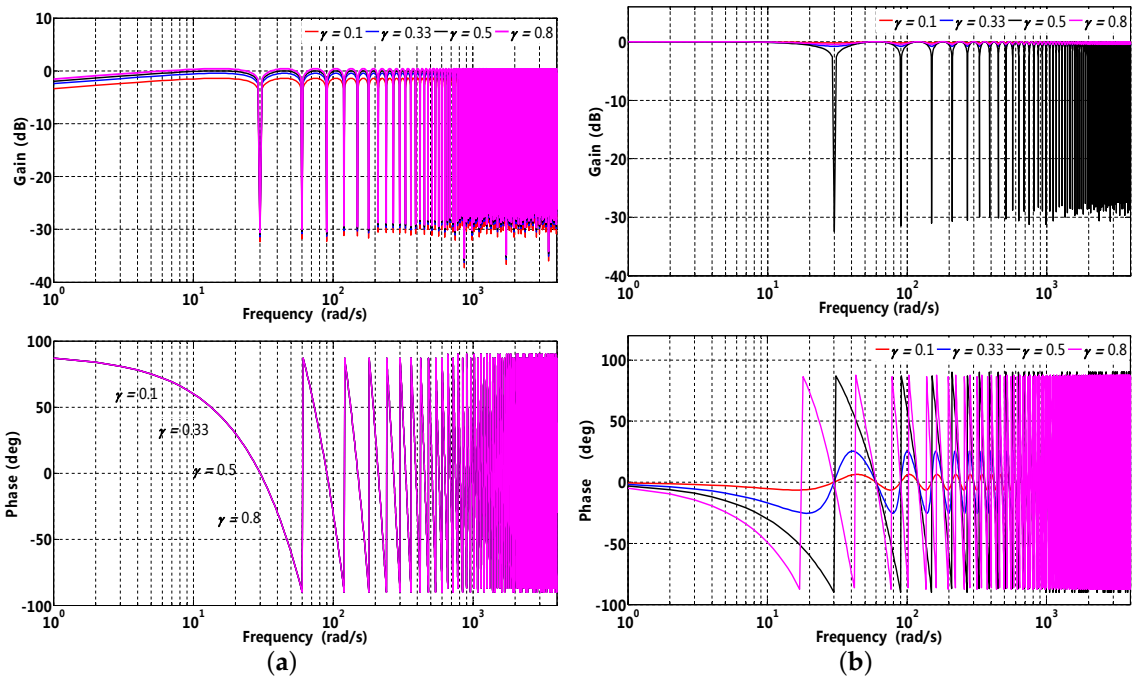

Figure 7. Frequency characteristics with respect to parameter γ: (**a**) $1 - Q(z^{-1})z^{-m}$; (**b**) $Q(z^{-1})$.

3.5. Robust Stability

For multiplicative uncertainty $\Delta(z^{-1})$, according to the small gain theorem [25], robust stability is guaranteed by the equivalent block diagram presented in Figure 4c. Supposing that $\Delta(z^{-1})$ is stable and bounded with H_∞ norm, robust stability must be satisfied as follows:

$$\left\| \Delta(z^{-1}) T(z^{-1}) \right\|_\infty < 1 \tag{21}$$

where the complementary sensitivity function can be obtained as follows:

$$T(z^{-1}) = \frac{PCz^{-m} + PP_n^{-1}Qz^{-m}}{1 + PCz^{-m} + (PP_n^{-1} - 1)Qz^{-m}} \tag{22}$$

3.6. Comparisons of PDOB with General DOB

The effectiveness of PDOB and general DOB are compared and analyzed in this section, primarily consisting of two parts: one is the effectiveness of different filters (LPF and ZPF) on PDOB, and the other is a comparison analysis with respect to general DOB and PDOB. Equations (11) and (10) represent disturbance suppression performance and robust stability, respectively. The frequency characteristics of PDOB with LPF, ZPF and general DOB are presented in Figure 8, where the corresponding parameters are $T_s = 0.1$ ms, $\omega_0 = 60$ rad/s, $\gamma = 0.5$, $g = 2000$ rad/s, respectively; the cutoff frequencies of DOB1 and DOB2 are 25 and 100 rad/s, respectively. In Figure 8a, the PDOB with $q(j\omega) = 1$ has a stronger disturbance suppression characteristic at harmonic frequency, which is composed of a fundamental frequency of 60 rad/s and harmonic frequencies at 120, 180, $\cdots$ rad/s. Moreover, PDOB with ZPF and LPF has almost the same magnitude gain in the low-frequency range, while the frequency mismatch caused by LPF phase delay can cause the harmonic disturbance suppression to deviate; meanwhile, in the high-frequency range, PDOB with ZPF hasa weaker disturbance suppression characteristic than that of LPF, which means that sensitivity and complementary sensitivity reach a compromise with each other. With regards to general DOB, the stronger disturbance characteristic (including periodic and aperiodic) in the low-frequency range illustrates that general

DOB is inappropriate for periodic disturbance suppression. In Figure 8b, PDOB with ZPF and LPF has a smaller magnitude gain at frequencies of 30, 90, 150, $\cdots$ rad/s; meanwhile, the magnitude gain at frequencies of 60, 120, 180, $\cdots$ rad/s are approximate to 0 dB, which can directly feedback to disturbance compensation and corresponds to the analyses in Equation (18). In addition, in the high-frequency range, measurement noise and harmonic components can be attenuated to break off disturbance compensation for closed loop robust stability. For general DOB, all the components (including periodic and aperiodic) are directly fed-back to compensate disturbance, which can deteriorate the disturbance suppression performance. Therefore, PDOB with ZPF has preferable disturbance suppression and noise sensitivity performance; meanwhile, PDOB with ZPF achieves a compromise between sensitivity and complementary sensitivity, allowing the realization of an optimal filter state [26].

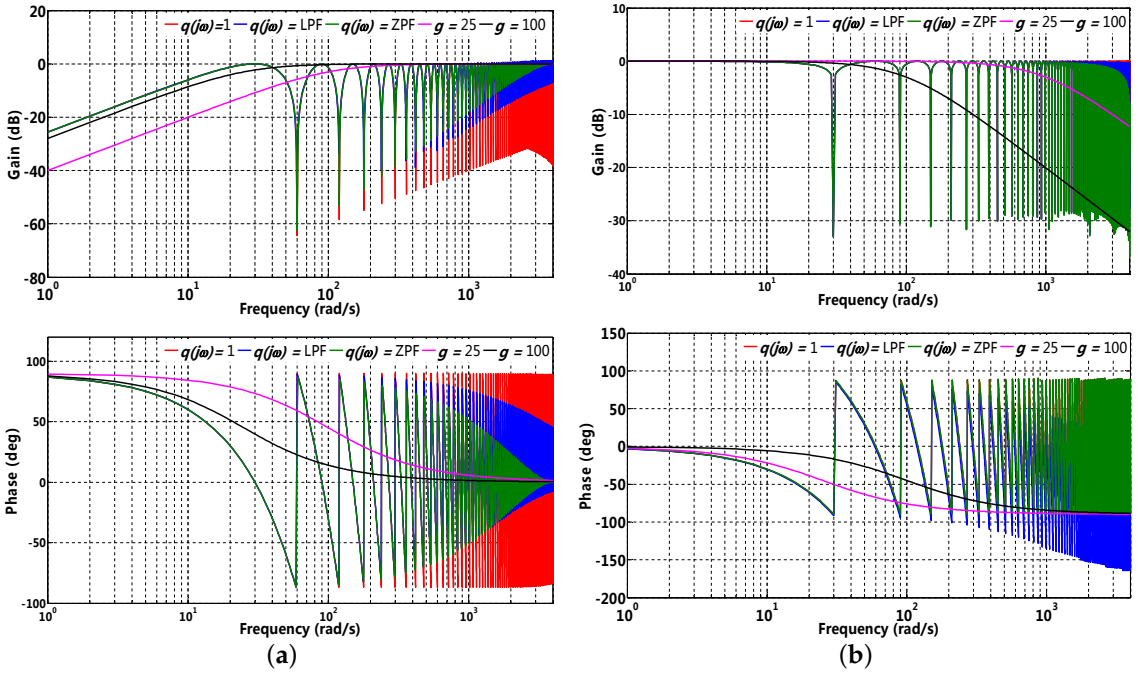

Figure 8. Frequency characteristics with respect to general DOB and PDOB: (**a**) $1 - Q(z^{-1})z^{-m}$; (**b**) $Q(z^{-1})$.

4. Adaptive Periodic Disturbance Observer

4.1. Fundamental Frequency Estimation

The algorithm of ANF frequency estimation based on the SM method is presented in Table 1. Where the estimation value of the fundamental frequency can be derived as $\hat{\omega} = \cos^{-1}(-0.5\hat{\theta})/T_s$, Δ denotes the delay parameter, which is employed to attenuate the correlation between $\tilde{d}(n)$ and $\tilde{d}(n-\Delta)$. λ, generally referred to the forgetting factor, increases to λ_∞ at the geometric ratio of λ_r; similarly, ρ, generally referred to the notch filter parameter of ANF, increases to a final value of ρ_∞ in the same way. The magnitude gain of the notch filter with respect to ρ is presented Figure 9; it can be seen that a larger value can enhance the frequency estimation convergence ratio. However, a fast convergence ratio may lead to an obvious transient overshoot or undershoot in frequency estimation; consequently, the response ratio and notch filter characteristic should reach a compromise to smooth the frequency estimation process. The Newton least mean square (Newton-LMS) method is substituted by normalized LMS (NLMS) to reduce the computational burden in this paper; in addition, the regular parameter δ is introduced to avoid numerical divergence in matrix inversion.

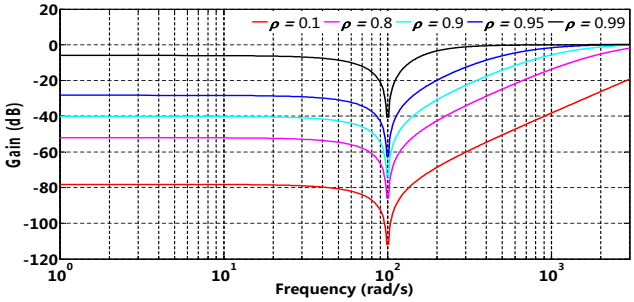

Figure 9. Magnitude gain of notch filter with respect to parameter ρ.

The second-order generalized integrator (SOGI) presented in Figure 10 can realize frequency tracking according to the internal model theorem, where the corresponding parameters are $T_s = 0.1$ ms and $\omega_0 = 20$ rad/s, which can be employed to extract the fundamental wave $\tilde{d}$ from the periodic disturbance ε, and the transfer functions can be derived as follows.

$$\begin{cases} D(s,\omega_0) = \dfrac{\tilde{d}}{\varepsilon} = \dfrac{b_p\omega_0 s}{s^2 + b_p\omega_0 s + \omega_0^2} \\ Q(s,\omega_0) = \dfrac{q\tilde{d}}{\varepsilon} = \dfrac{b_p\omega_0^2}{s^2 + b_p\omega_0 s + \omega_0^2} \end{cases} \tag{23}$$

SOGI is essentially a band pass filter (BPF) whose quality factor is $Q_D = 1/b_p$, which is free of other parameters and can effectively filter out fundamental components from periodic disturbance; however, the quality factor of general BPF is generally determined by the central frequency and bandwidth parameter b_p and is variable with frequency. Moreover, the phase of $q\tilde{d}$ lags behind that of $\tilde{d}$ by 90°, which can be employed to realize frequency tracking. It is observed that when the fundamental frequency of periodic disturbance varies, the frequency obtained by SOGI can be chosen as the resonant frequency; therefore, SOGI has a frequency adaptiveness characteristic. The frequency characteristics of $D(j\omega,\omega_0)$ are presented in Figure 11. It is clear that b_p presents decreasing results in terms of a remarkable narrowing of the pass band. When the harmonic components of periodic disturbance are comparably rich, a smaller value of b_p should be chosen, while the response ratio will slow down; therefore, a compromise should be reached between the bandwidth and response ratio to realize an optimal filter state.

From the analyses mentioned above, it is clear that periodic disturbance is variable under different operation environments; moreover, periodic disturbance suppression performance is variable with the fundamental frequency [27–29]. Therefore, fundamental frequency estimation is a critical part of realizing adaptive PDOB, which is estimated by ANF based on the SM method in this paper [23,24,30]. The control block diagram of adaptive PDOB is presented in Figure 12.

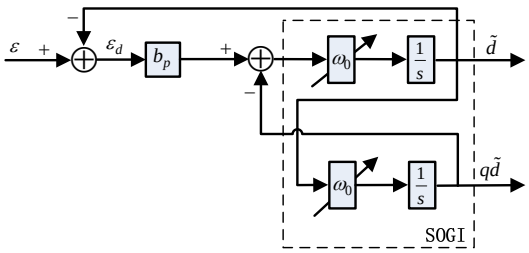

Figure 10. Control block diagram of the second-order generalized integrator (SOGI).

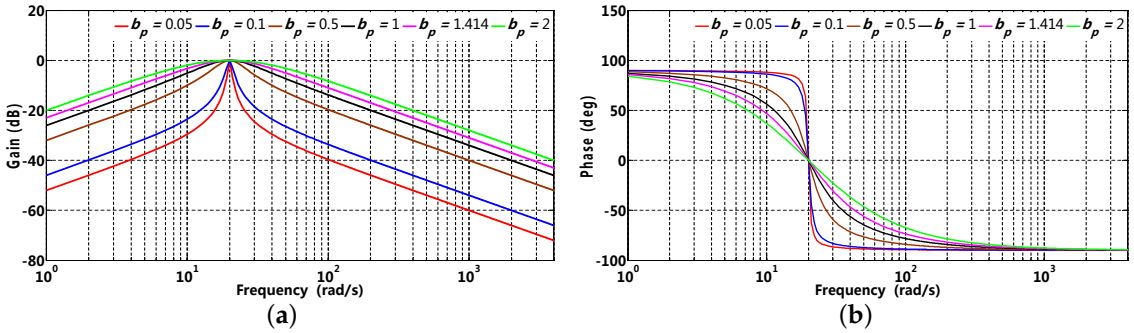

Figure 11. Frequency characteristics of SOGI with respect to parameter b_p: (**a**) magnitude; (**b**) phase.

Table 1. Adaptive notch filter (ANF) multi-frequency estimation algorithm based on SM method [23].

Input : m, Δ, λ, λ_r, λ_∞, ρ, ρ_r, ρ_∞, δ, μ
Nominal values: $\lambda = 0.65$, $\lambda_r = 0.99$, $\lambda_\infty = 0.995$
$\rho = 0.65$, $\rho_r = 0.99$, $\rho_\infty = 0.995$, $\delta = 0.001$, $\mu = 0.3$
$\hat{\theta}(-1) = [0, \cdots, 0]^{\mathrm{T}}$
$h(i) = g(i) = 0$ for $i = -2m, \cdots, -1$
Main iteration loop : for $n = 0, \cdots, N$
define : $a = \sum_{i=1}^{m-1} \left[\rho^i g(n-i) + \rho^{2m-i} g(n-2m+i)\right] \hat{a}_i(n-1)$
define : $b = \sum_{i=1}^{m-1} \left[\rho^i h(n-i) + \rho^{2m-i} h(n-2m+i) \hat{a}_i(n-1)\right]$
$g(n) = \tilde{d}(n) - \rho^{2m} g(n-2m) - a - \rho^m g(n-m) \hat{a}_m(n-1)$
$h(n) = \tilde{d}(n-\Delta) - \rho^{2m} h(n-2m) - b - \rho^m h(n-m) \hat{a}_m(n-1)$
$\Phi(n) = [\phi_1(n), \phi_2(n), \cdots, \phi_m(n)]^T$
Adaptive algorithm:
$e(n) = g(n-\Delta+1) + \rho^{2m} g(n-2m-\Delta+1) - (\rho^{2m}-1) h(n-2m+1) - \Phi^T(n) \hat{\theta}(n-1)$
$\hat{\theta}(n) = \hat{\theta}(n-1) + \frac{\mu}{\delta + \Phi^T(n)\Phi(n)} \Phi(n) e(n)$
$\lambda = \lambda_r \lambda + (1-\lambda_r) e(n)$
$\rho = \rho_r \rho + (1-\rho_r) e(n)$
Fundamental frequency:
$\hat{\omega}_i(n) = \cos^{-1}(-0.5 \hat{\theta}_i(n)) / T_s$

4.2. Parameter Design

When estimating the fundamental frequency of periodic disturbance, the delay parameter Δ, bandwidth parameter b_p of $D(s, \hat{\omega}_0)$ and cutoff frequency g_a of $q_a(z^{-1}) = g_a/(j\omega + g_a)$ need to taken into consideration. In order to demonstrate their influences on frequency estimation, two different frequencies are estimated simultaneously by ANF based on the SM method.

$$f_1(t) = \begin{cases} 1.5 \text{ rad/s} & 0 < t \le 6 \text{ s} \\ 2 \text{ rad/s} & 6 < t \le 20 \text{ s} \end{cases}, \quad f_2(t) = \begin{cases} 1 \text{ rad/s} & 0 < t \le 6 \text{ s} \\ 1.2 \text{ rad/s} & 6 < t \le 20 \text{ s} \end{cases} \tag{24}$$

Colored noise $e(n)$ with a signal-to-noise ratio (SNR) of $1/0.04$ is output from the AR(1) model with the transfer function $1/(1-0.7z^{-1})$. The frequency estimation waveforms with respect to the delay parameter are presented in Figure 13a. It can be observed that, for $\Delta = 2$, colored noise makes the frequency estimation biased owing to the correlation between $\tilde{d}(n)$ and $\tilde{d}(n-\Delta)$; for $\Delta = 15$, a weak correlation between $\tilde{d}(n)$ and $\tilde{d}(n-\Delta)$ improves the frequency estimation precision. Meanwhile, when the reference frequency suddenly changes, the frequency estimation waveform can realize fast tracking without great overshoot or undershoot. Therefore, a proper delay parameter can reduce the correlation owing to colored noise contamination to improve frequency estimation precision.

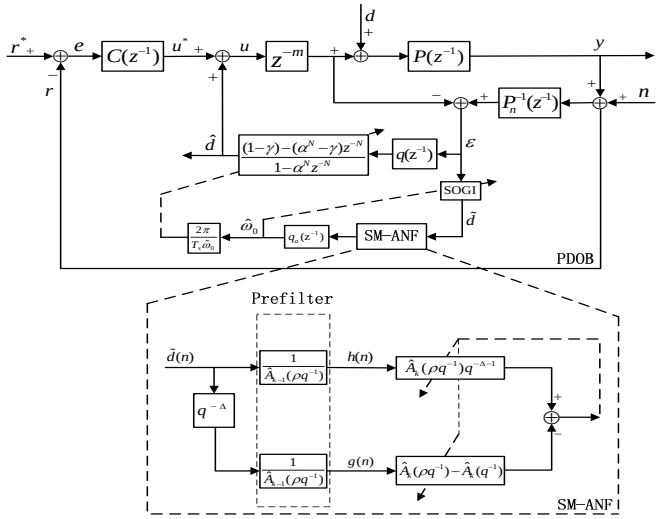

Figure 12. Block diagram of adaptive PDOB based on the Stieglitz–McBride (SM) method.

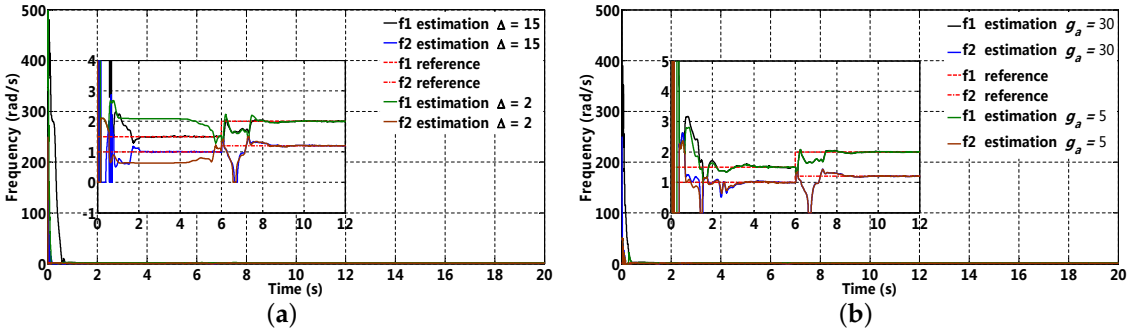

Figure 13. Frequency estimation with respect to parameter Δ and g_a: (**a**) parameter Δ; (**b**) parameter g_a.

The cutoff frequency g_a is employed to attenuate the transient overshoot or undershoot presented in Figure 13b; it can be observed that for $g_a = 30$, frequency estimation exhibits an obvious overshoot in the beginning, and it takes almost 2 s to track the reference frequency. In contrast, for $g_a = 5$, the frequency estimation waveform becomes comparably smooth without a great overshoot in the beginning and sudden frequency variation. Therefore, an appropriate selection of the cutoff frequency g_a can smooth the frequency estimation procedure to avoid overshoot or undershoot.

5. Simulations and Experiments

5.1. Simulation

Fundamental frequency estimation is critical to implement APDOB, as analyzed above. In order to demonstrate the feasibility and effectiveness of the proposed method, a MATLAB simulation based on an original PI controller (without disturbance compensation), general DOB, PDOB and APDOB are constructed, respectively; moreover, the corresponding speed and q-axis current are provided, and the simulation parameters are presented in Table 2.

Table 2. Simulation parameters.

Parameter	Symbol	Value
Sampling time	T_s	0.01 ms
Cutoff frequency of $q_a(z^{-1})$	g_a	10 rad/s
Cutoff frequency of PDOB	g	1000 rad/s
Cutoff frequency of general DOB	g_{dob}	1000 rad/s
Delay parameter	Δ	15
Bandwidth of SOGI	b_p	0.1
α initial value	α_{init}	0.8
α geometry ratio	α_r	0.95
α final value	α_∞	0.99
Design parameter	γ	0.5
Convergence ratio	μ	0.3
Stator winding resistance	R_s	2.875 Ω
d-axis inductance	L_d	0.0085 H
q-axis inductance	L_q	0.0119 H
Flux	ψ_m	0.175 Wb
Moment of inertia	J_n	0.003 kg $\cdot$ m^2
Pole pairs	n_p	3
Electromagnetic torque constant	K_{Tn}	0.525 Nm/A
DC bus voltage	V_{dc}	310 V

Where 400 r/min (20 Hz) is selected as a reference to intuitively reflect the speed fluctuation suppression performance, fundamental frequency and periodic disturbance (consisting of fundamental wave and harmonic components), which are defined as follows.

$$f_0 = \begin{cases} 10\text{ Hz} & 0 < t \le 8\text{ s} \\ 14\text{ Hz} & 8 < t \le 18\text{ s} \end{cases}, \quad \begin{cases} A_p = \begin{bmatrix} 2 & 0.4 & 0.6 & 0.8 & 0.2 & 1.2 \end{bmatrix} \\ d_p = \sum_{n=1}^{6} A_p(n) \sin(n\omega_0 T_s t) \end{cases} \tag{25}$$

The fundamental frequency estimation waveform of APDOB is presented in Figure 14; it can be observed that the estimation value remains constant in the beginning, where 4 Hz is selected as an initial value to avoid estimation instability. When the reference frequency varies suddenly, frequency estimation can track the reference value with a smaller overshoot and shorter adjusting time; in addition, a small estimation deviation in a steady state (no more than 0.15 Hz) is satisfied with practical requirements, which can lay a solid foundation to realize the frequency adaptiveness of PDOB.

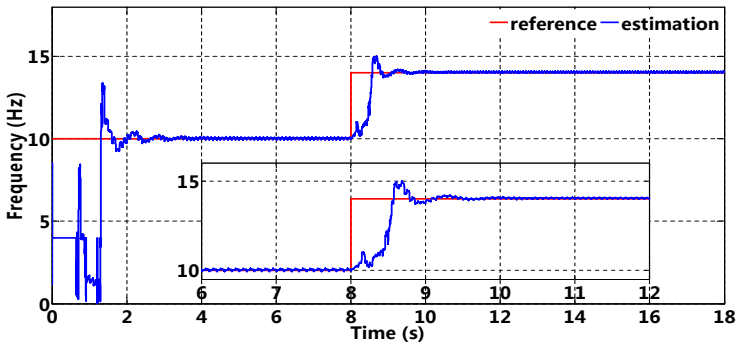

Figure 14. Fundamental frequency estimation.

The speed and corresponding q-axis current based on the original PI controller (without disturbance compensation), DOB, PODB and APDOB are presented in Figure 15, where the left and right halves represents the speed and corresponding q-axis current waveform, respectively. Figure 15a,b

represents the speed and corresponding q-axis with an original PI controller; it can be observed that speed has an apparent fluctuation. Similarly, the q-axis current also has an apparent fluctuation, which is primarily caused by periodic disturbance. Figure 15c,d represents the speed and corresponding q-axis current with DOB; all disturbance components within the cutoff frequency (including periodic and aperiodic) can be employed to q-axis current compensation, although speed fluctuation can be suppressed to some extent (no more than 20 r/min), and finite sensitivity gain at disturbance-related frequencies cannot further enhance the speed fluctuation suppression performance. Figure 15e,f represents the speed and corresponding q-axis current with PDOB. It can be observed that speed fluctuation can be effectively suppressed before disturbance fundamental frequency variation, however, which results in a larger speed fluctuation after the disturbance of the fundamental frequency variation; in particular, closed loop system stability may be destroyed. Figure 15g,h represents the speed and corresponding q-axis current with APDOB and the apparent speed fluctuation in transient stage (speed up) owing to frequency estimation deviation; it takes 2 s to recover its steady state, meanwhile, leading to a smaller speed fluctuation (no more than 10 r/min). A similar phenomenon can also occur when the fundamental frequency changes suddenly It can be observed that the fundamental frequency estimation, as shown in Figure 14, achieves its steady state in 3 s, which illustrates that speed fluctuation based on current compensation has a faster response ratio compared with that of direct speed compensation. Through the analyses mentioned above, speed fluctuation can be effectively suppressed with APDOB owing to the sufficient sensitivity gain at the fundamental and its harmonic frequencies compared with that of DOB, while an apparent speed fluctuation can occur after frequency variation for PDOB owing to its lack of frequency adaptiveness. Therefore, speed fluctuation suppression performance can be guaranteed by frequency adaptiveness based on ANF, while PDOB cannot guarantee this.

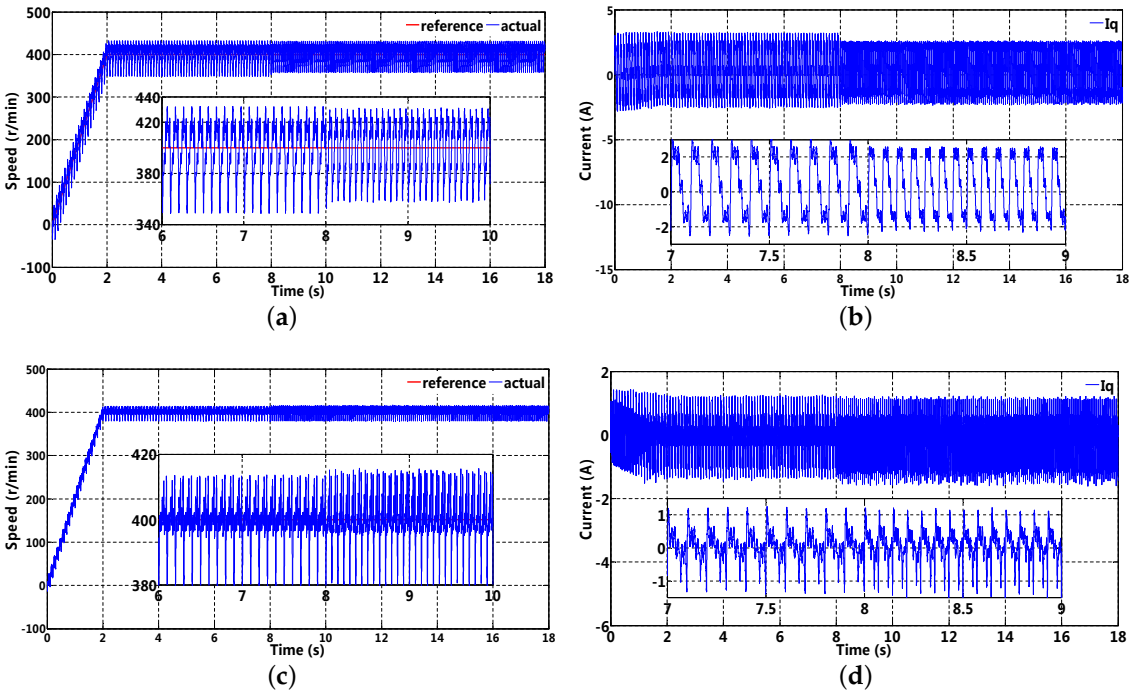

Figure 15. *Cont.*

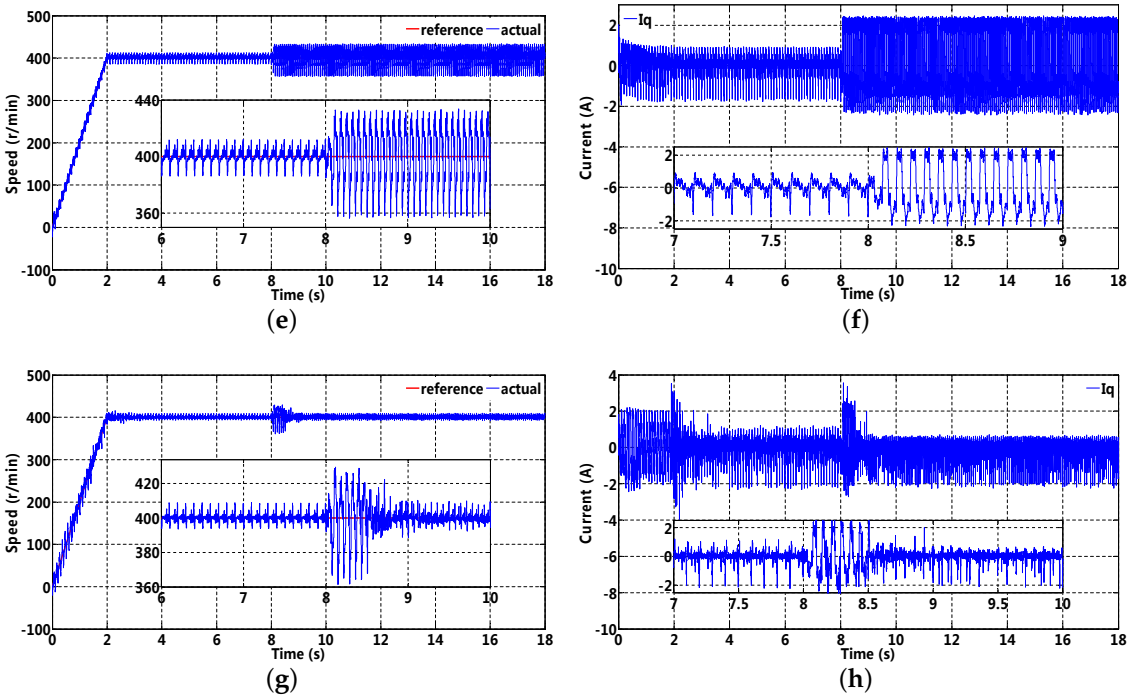

Figure 15. Speed and corresponding q-axis current based on the original PI controller (without disturbance compensation), DOB, PDOB and APDOB: (**a**,**b**) speed and corresponding q-axis current with the original PI controller; (**c**,**d**) speed and corresponding q-axis current with DOB; (**e**,**f**) speed and corresponding q-axis current with PDOB; (**g**,**h**) speed and corresponding q-axis current with APDOB.

5.2. Experiment Setup

The nominal parameters of the inverter compressor are presented in Table 3. In order to validate the effectiveness of the proposed scheme, experiments were implemented on the inverter compressor platform presented in Figure 16, where the floating point TI DSP TMS320F28069 (TX) was selected as the micro-processor, sampling and pulse width modulation (PWM) switching frequency are set to 10 KHz. Moreover, the current, voltage and speed base value are chosen as $5.2 \times \sqrt{2}$ A, 310 V and 3000 r/min (considering flux weakening range), respectively.

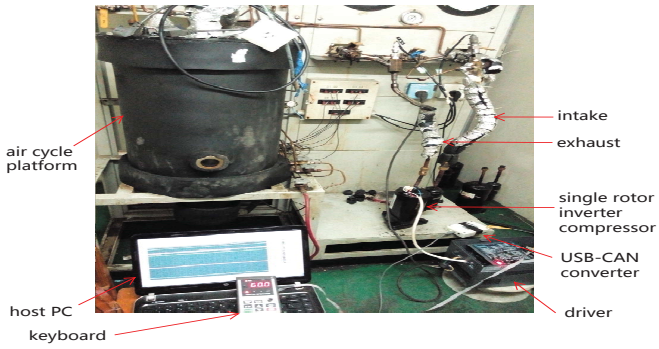

Figure 16. Experimental platform of inverter compressor.

Table 3. Experimental parameters.

Parameter	Symbol	Value
Pole pairs	n_p	3
Stator resistance	R_s	1.47 Ω
d-axis inductance	L_d	6.87 mH
q-axis inductance	L_q	9.31 mH
Flux	ψ_m	345 mWb
back EMF constant	K_v	39.2 V/krpm
Electromagnetic torque constant	K_{Tn}	0.46 Nm/A
Moment of inertia	J_n	310 Kg·mm^2
Rated current	I_n	5.2 A (60 Hz)
Rated frequency	f	60 Hz
Cutoff frequency of PDOB	g	1000 rad/s
Cutoff frequency of DOB	g_{dob}	1000 rad/s
Cutoff frequency of $q_a(z^{-1})$	g_a	5 rad/s
Delay parameter	Δ	20
Bandwidth of SOGI	b_p	0.1
α initial value	α_{init}	0.8
α geometry ratio	α_r	0.95
α final value	α_∞	0.99
Design parameter	γ	0.5
Convergence factor	μ	0.3

The speed and corresponding q-axis current at 15 Hz are presented in Figure 17, which could be obtained in real-time using a USB–CAN converter linked to a host computer. It is clear that the q-axis current in Figure 17b has a large fluctuation caused by the approximately periodic disturbance; consequently, an apparent speed fluctuation is present for the original PI controller (no more than 25 r/min), which could possibly deteriorate the normal operation of the inverter compressor, especially its self-sensing control. Although speed fluctuation can be suppressed to some extent (no more than 7 r/min), the q-axis current in Figure 17d presents periodicity to some extent, which may be the result of the following factors: firstly, the finite sensitivity gain of the Q filter cannot effectively realize periodic disturbance suppression; secondly, the small cutoff frequency of the LPF can increase sensitivity gain, while the apparent phase lag can reduce the current compensation performance. Periodic components of the q-axis current can be observed in Figure 17f and could be effectively compensated, except for some aperiodic components, in agreement to the assumptions mentioned above; moreover, a small speed deviation can be obtained with APDOB (no more than 2 r/min). Similar results are also shown in Figure 18 under almost the same operation environment. In Figure 18b, the q-axis current presents a certain periodicity without disturbance compensation and an obvious speed fluctuation is present (nomore than 25 r/min), while in Figure 18f, periodic components of q-axis current could be effectively compensated with APDOB, except for some aperiodic components. In addition, a smaller speed fluctuation (no more than 2 r/min) could be obtained when compared with that of DOB (no more than 7 r/min).

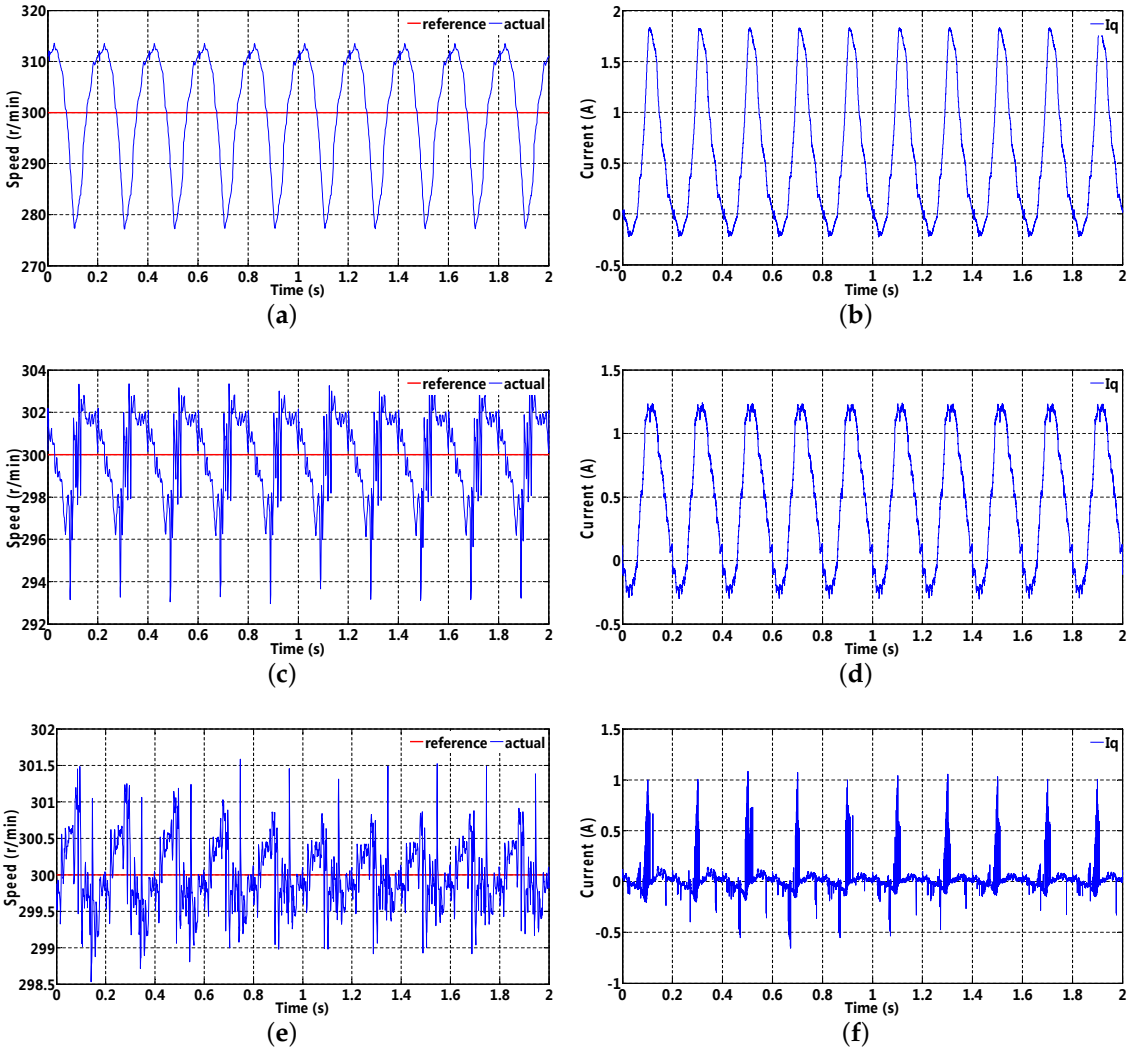

Figure 17. Speed and corresponding q-axis current based on the original PI controller (without disturbance compensation), DOB and APDOB (15 Hz): (**a**,**b**) speed and corresponding q-axis current with the original PI controller; (**c**,**d**) speed and corresponding q-axis current with DOB; (**e**,**f**) Speed and corresponding q-axis current with APDOB.

In order to clearly reflect speed fluctuation suppression performance, the root mean square error (RMSE) criterion is employed, and the speed fluctuation ratio Δ_{spd} can be expressed as follows.

$$\Delta_{spd} = \sqrt{\frac{1}{m}\sum_{i=1}^{m}\left(\frac{\omega_m(i)}{\omega_m^*} - 1\right)^2} \tag{26}$$

where $m = n_p/(fT_{spd})$, f, ω_m^* and ω_m denote sampling number, operation frequency, reference and actual speed, respectively, T_{spd} denotes sampling time of speed loop and 1 ms is selected in this paper. Speed fluctuation ratio and corresponding speed error are presented in Table 4, it can be observed that speed fluctuation becomes large with frequency decreasing under almost same operation environment, in addition, comparably smaller speed fluctuation ratio can be obtained owing to larger reference value, which illustrates that speed fluctuation in low frequency range should be primarily taken into consideration. In consequently, speed fluctuation suppression based on APDOB is feasible and effective in low frequency range for inverter compressor.

Table 4. Speed fluctuation ratio and corresponding error.

Method	15 Hz	20 Hz
PI	5.8%	4.5%
	17.4 r/min	18.1 r/min
DOB	1.5%	1.3%
	4.7 r/min	5.3 r/min
APDOB	0.6%	0.4%
	1.8 r/min	1.6 r/min

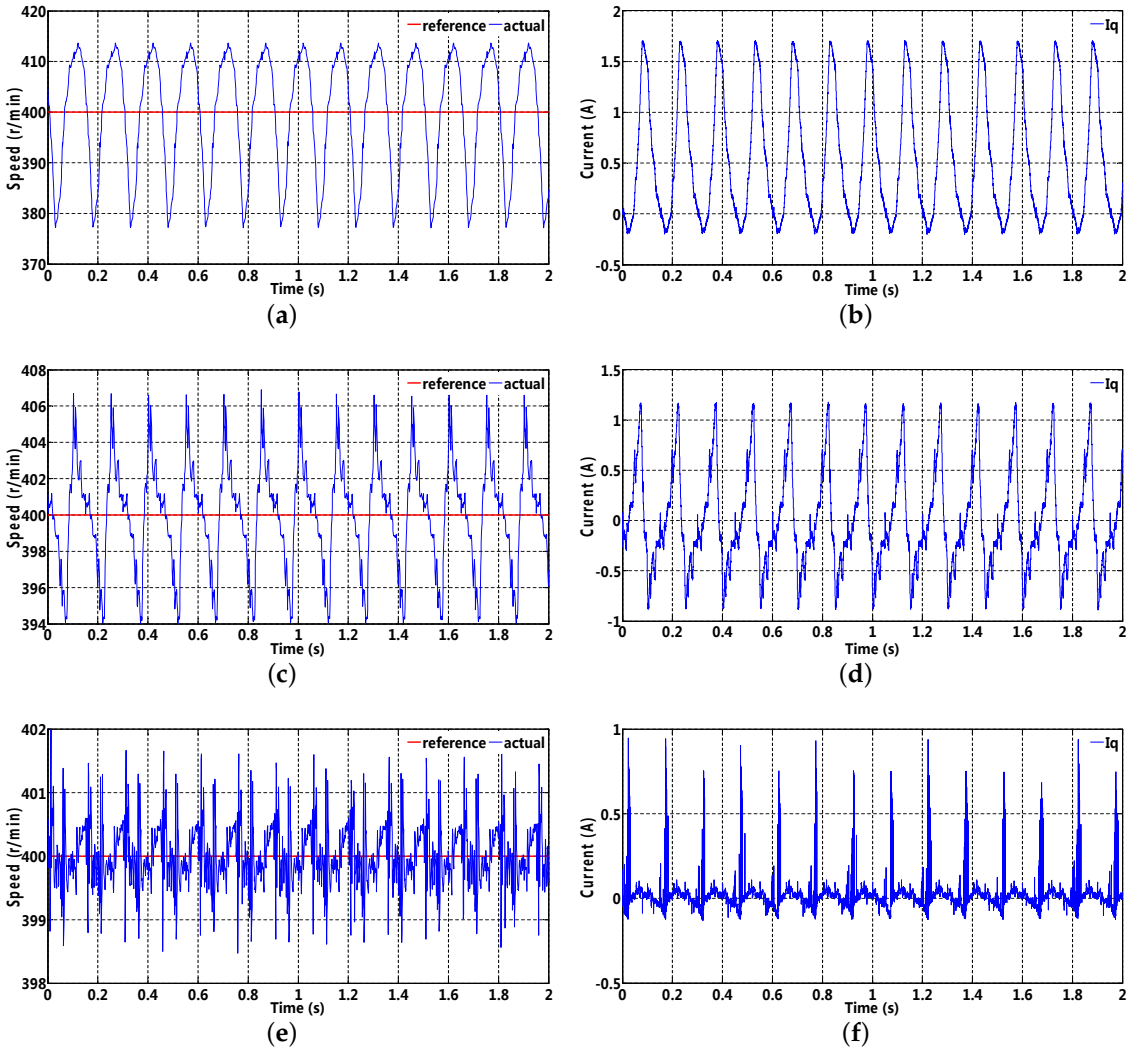

Figure 18. Speed and corresponding q-axis current based on the original PI controller (without disturbance compensation), DOB and APDOB (20 Hz): (**a**,**b**) speed and corresponding q-axis current with the original PI controller; (**c**,**d**) speed and corresponding q-axis current with DOB; (**e**,**f**) speed and corresponding q-axis current with APDOB.

6. Conclusions

In order to attenuate the speed fluctuation of an inverter compressor in the low-frequency range, adaptive PDOB is adopted in this paper. Firstly, PDOB is constructed, and corresponding parameters are analyzed and designed, although sensitivity and complementary sensitivity can reach

a compromise through the use of parameter γ. However, the fractional delay item cannot be corrected by ZPF and needs to be optimized in the future. Secondly, SOGI is adopted to filter out fundamental waves, and ANF based on the SM method is proposed to estimate the fundamental frequency of periodic disturbance. Thirdly, MATLAB simulations and experiments are implemented to validate the feasibility and effectiveness of APDOB, respectively. It should be noted that an appropriate selection of cutoff frequency to achieve a compromise between sensitivity and complementary sensitivity should be taken into consideration in practical application. The experimental results illustrate that, compared with DOB, the speed fluctuation of an inverter compressor can be effectively suppressed by APDOB in the low-frequency range.

Author Contributions: Writing—original, software and methodology, F.M.; validation, X.W.; formal analysis and resource, X.S.; conceptualization, F.M.; writing—review and editing, Z.L., M.N. and L.Y.; funding acquisition, Z.L. All authors have read and agreed to the published version of the manuscript.

Funding: This research was funded by the "National Natural Science Foundation of China, grant number 51707014", "GuangDong Province Natural Science Foundation, grant number 2019A1515011041" and "Shenzhen Science and Technology Innovation Commission International Cooperation Research, grant number GJHZ20190819152001781".

Acknowledgments: The authors thank all of reviewers for their insights and suggestions, which are very helpful to this manuscript improvements.

Conflicts of Interest: All authors have no conflict of interest.

References

1. Zhang, G.Z. The Method that Speed Suppression of Inverter Compressor Based on Fourier Transformation. In Proceedings of the IECON 2013 Conference of China HouseHold Appliance Technology, Wuxi, China, 24–26 October 2013; pp. 491–496. [CrossRef]
2. Huang, H.; Ma, Y.J.; Zhang, Y.L. The Method that Reducing Speed Fluctuation of Single Rotor Inverter Compressor in Air-conditioner. *J. Electr. Mach. Control.* **2011**, *15*, 98–102. [CrossRef]
3. Chen, W.H.; Yang, J.; Guo, L. Disturbance Observer-Based Control and Related Methods: An Overview. *IEEE Trans. Ind. Electron.* **2016**, *63*, 1083–1095. [CrossRef]
4. Ohnishi, K.; Shibata, M.; Murakami, T. Motion control for advanced mechatronics. *IEEE-ASME Trans. Mechatron.* **1996**, *1*, 56–67. [CrossRef]
5. Cho, K.; Kim, J.; Choi, S.B.; Oh, S. A high-precision motion control based on a periodic adaptive disturbance observer in a PMLSM. *IEEE-ASME Trans. Mechatron.* **2015**, *20*, 2158–2171. [CrossRef]
6. Chen, X. New Repetitive Control With Improved Steady-State Performance and Accelerated Transient. *IEEE Trans. Control Syst. Technol.* **2014**, *22*, 664–675. [CrossRef]
7. Lin, F.J.; Chou, P.H.; Kung, Y.S. Robust fuzzy neural network controller with nonlinear disturbance observer for two-axis motion control system. *IET Control Theory Appl.* **2008**, *2*, 151–167.
8. Muramatsu, H.; Katsura, S. An Adaptive Periodic-Disturbance Observer for Periodic-Disturbance Suppression. *IEEE Trans. Ind. Inform.* **2018**, *14*, 4446–4456. [CrossRef]
9. Han, J.Q. Extended state observer for a class of uncertain plants. *China Control Des.* **1995**, *10*, 85–88. [CrossRef]
10. Huang, Y.; Xue, W.C. Active disturbance rejection control: Methodology, application and theoretical analysis. *ISA Trans.* **2014**, *53*, 963–976. [CrossRef]
11. Hara, S.; Yamamoto, Y.; Omata, T.; Nakano, M. Repetitive control system: A new type servo system for periodic exogenous signals. *Int. J. Robust Nonlinear Control* **1988**, *33*, 659–668. [CrossRef]
12. Francis, B.A.; Wonham, W.M. The internal model principle for linear multivariable regulators. *Appl. Math. Optim.* **1975**, *2*, 170–194. [CrossRef]
13. Zhang, M.; Huang, L.; Yao, W.; Lu, Z. Circulating harmonic current elimination of a CPS-PWM-based modular multilevel converter with a plug-in repetitive controller. *IEEE Trans. Power Electron.* **2013**, *29*, 2083–2097. [CrossRef]
14. Tsai, M.C.; Yao, W.S. Design of a plug-in type repetitive controller for periodic inputs. *IEEE Trans. Control Syst. Technol.* **2002**, *10*, 547–555. [CrossRef]

15. Jin, W.; Li, Y.; Sun, G.; Bu, L. H∞ Repetitive Control Based on Active Damping with Reduced Computation Delay for LCL-Type. *Energies* **2017**, *10*, 586–604. [CrossRef]
16. Chung, C.H.; Chen, M.S. A robust adaptive feedforward control in repetitive control design for linear systems. *Automatica* **2015**, *48*, 183–190. [CrossRef]
17. Pipeleers, G.; Demeulenaere, B.; De Schutter, J.; Swevers, J. Robust High-Order Repetitive Control. *Automatica* **2008**, *44*, 2628–2634. [CrossRef]
18. Cui, P.; Li, S.; Zhao, G.; Peng, C. Suppression of Harmonic Current in Active-Passive Magnetically Suspended CMG Using Improved Repetitive Controller. *IEEE-ASME Trans. Mechatron.* **2016**, *21*, 2132–2141. [CrossRef]
19. Cui, P.; Wang, Q.; Li, S.; Gao, Q. Combined FIR and Fractional-Order Repetitive Control for Harmonic Current Suppression of Magnetically Suspended Rotor System. *IEEE Trans. Ind. Electron.* **2017**, *64*, 4828–4835. [CrossRef]
20. Chen, D.; Zhang, J.M.; Qian, Z.M. An Improved Repetitive Control Scheme for Grid-Connected Inverter with Frequency-Varying Adaptability. *IEEE Trans. Ind. Electron.* **2013**, *60*, 814–823. [CrossRef]
21. Lu, Y.S.; Lin, S.M.; Hauschild, M.; Hirzinger, G. A torque-ripple compensation scheme for harmonic drive systems. *IEEE Trans. Ind. Inform.* **2013**, *95*, 357–365.
22. Marino, R.; Tomei, P. Adaptive notch filters are local adaptive observers. *Int. J. Adapt. Control Signal Process.* **2015**, *30*, 128–146.
23. Cheng, M.H.; Tsai, J.L. A new IIR adaptive notch filter. *Signal Process.* **2006**, *86*, 1648–1655. [CrossRef]
24. Diniz, P. *Adaptive Filtering: Algorithms and Practical Implementation*; 4th ed.; Springer: New York, NY, USA, 2013. [CrossRef]
25. Doyle, J.C.; Francis, B.A.; Tannenbaum, A. *Feeeback Control Theory*; Courier Corporation: New York, NY, USA, 1992. [CrossRef]
26. Sariyildiz, E.; Ohnishi, K. Stability and Robustness of Disturbance-Observer-Based Motion Control Systems. *IEEE Trans. Ind. Electron.* **2014**, *62*, 414–422. [CrossRef]
27. Jafari, S.; Ioannou, P.; Fitzpatrick, B.; Wang, Y. Robustness and Performance of Adaptive Suppression of Unknown Periodic Disturbances. *IEEE Trans. Autom. Control* **2015**, *60*, 2166–2171.
28. Landau, I.D.; Constantinescu, A.; Alma, M. Adaptive regulation—Rejection of unknown multiple narrow band disturbances. *Control Eng. Pract.* **2011**, *19*, 1168–1181.
29. Jafari, S.; Ioannou, P.A. Rejection of unknown periodic disturbances for continuous-time MIMO systems with dynamic uncertainties. *Int. J. Adapt. Control Signal Process.* **2016**, *30*, 1674–1688.
30. Li, G. A stable and efficient adaptive notch filter for direct frequency estimation. *IEEE Trans. Signal Process.* **1997**, *45*, 2001–2009.